DOI: 10.1002/ ((please add manuscript number))
Article type: Full Paper

The effects of cesium ion implantation on the mechanical and electrical properties of porous SiCOH low-*k* dielectrics

Weiyi Li, Dongfei Pei, Daniel Benjamin, Jen-Yung Chang, Sean W. King, Qinghuang Lin, and J. Leon Shohet*

W. Li, Dr. D. Pei, D. Benjamin, Dr. J.-Y. Chang, Prof. J.L. Shohet
Plasma Processing and Technology Laboratory, Department of Electrical and Computer Engineering, University of Wisconsin-Madison, Madison, Wisconsin 53706, USA
*Email: shohet@engr.wisc.edu

Dr. J.-Y. Chang, Dr. S. W. King
Intel Corporation, Hillsboro, Oregon 97124, USA

Dr. Q. Lin
IBM T.J. Watson Research Center, Yorktown Heights, New York 10598, USA

Keywords: low-*k* dielectrics, heavy-ion implantation, *k*-values, elastic moduli, curing

Abstract

In this work, we report an investigation of the effects of cesium (Cs) ion implantation on both porogen-embedded and UV-cured (porous) SiCOH films. For porogen-embedded SiCOH, it was found that Cs ion implantation can greatly improve the elastic modulus. It can also increase the time-zero dielectric breakdown (TZDB) strength. It also leads to an increase in the *k*-value for of medium and high Cs doses, but for low Cs doses the *k*-value decrease compared with its pristine counterpart. For UV-cured SiCOH, it was found that Cs ion implantation does not improve the elastic modulus. It also leads to lower TZDB field strength and much higher *k*-values than its pristine counterpart. These effects can be understood by examining the changes in chemical bonds. This treatment is shown to have a potential to help solve the problem between the demand for lower *k*-values and the concomitant weak mechanical strength of SiCOH.

1 Introduction

Being a part of solving the huge puzzle that extends Moore's Law,[1] low dielectric constant (low-*k*-value, or low-*k*) materials are being used to replace SiO_2 in back-end-of-line (BEOL) interconnections.[2] It is important to reduce the resistance-capacitance delay (RC-delay) in the interconnects, which increases as the critical-dimension scaling proceeds downwards.[2] Among some candidates for low-k interconnects,[3-8] organosilicate glass, which is often called SiCOH, SiOC, SiOCH, or SiOC:H, has been adopted for BEOL applications.[9-11] In order to push the *k*-value of these materials lower to meet the requirements of the international technology roadmap of semiconductor (ITRS),[12] porosities were introduced into these materials.[13-18] The currently dominant method to introduce porosity is by embedding a sacrificial porogen material during SiCOH film deposition, and then removal the porogen with a combination of thermal heating and ultra-violet (UV) light exposure.[14, 19-23] This combined treatment is usually referred to as UV-curing.[14, 19-23] A UV-cured SiCOH film is porous and thus has a lower *k*-value than its nonporous counterpart.

However, a problem with porous SiCOH (p-SiCOH) is that its mechanical properties, *e.g.* elastic modulus and hardness, can be greatly weakened because of the porosity. For example, the elastic modulus of p-SiCOH is 4-6 GPa while its nonporous counterpart shows values of 15-20 GPa.[24-26] For comparison, the elastic modulus of SiO_2 lies in the range of 57-92 GPa.[27] These weak mechanical properties may cause problems during CMP (chemical-mechanical polishing) and packaging.[28] A number of ways have been suggested to solve this problem.[29-31]

Our previous work[32] has shown that cesium (Cs) ion implantation in non-porous (no porogen involved) SiCOH low-*k* dielectric films can help improve its mechanical properties, including both the elastic modulus and hardness. The time-zero dielectric breakdown (TZDB) characteristics were also improved. However, along with these improvements, the Cs implanted material exhibited an increase in the *k*-value and loss of hydrophobicity.

In this work, we investigate the effects of Cs ion implantation on the mechanical and electrical properties of p-SiCOH dielectrics. In addition, the effects of thermal annealing after ion implantation are also investigated. The details of sample selection, Cs ion implantation specifications, and sample characterization methods will be discussed in Section 2. The measured data will be shown and discussed in Section 3.

2. Experiments

Two types of SiCOH films, named V1 and V2, are used in this work. They were provided by Intel. The properties of them are listed in **Table 1** below.

Table 1 Properties of SiCOH films used in this work

Film type	UV cured?	Thickness (nm)	*k*-value	Porosity
V1	No	226.8	2.8	Porogen embedded
V2	Yes	181.5	2.1	42%

Note that V1 has embedded porogens, and V2 is simply UV-cured V1.

The Cs ion-implantation conditions chosen for these samples are listed in **Table 2**. These

conditions were chosen based on an SRIM code simulation,[33] with the goal of keeping the Cs ion distribution centered roughly in the middle of the film thickness. Because of the porosity of the V2 film, Cs ions with the same kinetic energy can travel deeper into the film. And the effective concentration, taking into account porosity, would increase for the same dose, compared with the V1 film. Therefore, the ion energy and dose for the V2 film need to be reduced accordingly to achieve the same conditions as those for the V1 film.

Table 2 Ion implantation conditions. Labels: I-implanted, L-low dose, M-medium dose, H-high dose.

Film type	**Sample label**	**Ion Energy [keV]**	**Ion Dose [cm^{-2}]**
	V1-I-L	100	1×10^{13}
V1	V1-I-M	100	4×10^{13}
	V1-I-H	100	8×10^{13}
	V2-I-L	50	6×10^{12}
V2	V2-I-M	50	2.4×10^{13}
	V2-I-H	50	4.8×10^{13}

After implantation, all the samples were cut into two pieces, one of which was not processed further. These samples were labeled as implanted only. The other piece was annealed in a vacuum heater at 300°C for one hour and labeled as implanted and annealed. For comparison, samples of the *unimplanted* pristine films were also annealed in the same manner. Thus, there are four types of samples after this point: (1) pristine (P), (2) thermal-annealed only (A), (3) ion-implanted only (I), and (4) implanted-and-annealed (I-A). For both I and I-A samples three cesium doses were used, low (L), medium (M), and high (H) as shown in Table 2.

The film thickness of each sample was measured with a Rudolph AutoElII-VIS-3

ellipsometer. The ellipsometer beam incident angle was fixed at 70°. Three wavelengths 632.8 nm (R), 546.1 nm (G), and 405 nm (B) were selected for the incident beam for measurement and subsequent fitting.

The elastic modulus of each sample was measured using nanoindentation with a Hysitron TI 950 Triboindenter. A conventional Berkovich tip was used in such measurements. A comparison between measured effective moduli with a theoretical model developed by Stone[34] allows us to determine the elastic moduli for the low-k film itself.[26, 32]

The *k*-values of the films were determined from their C-V characteristics.[35] The setup for the C-V measurement utilizes a Signatone H-150W probe station with a 5-μm diameter pin probe, an HP 4285A LCR meter, and an MIS (metal-insulator-semiconductor) stack structure. The metal dots of the MIS structure are made with a silver (200 nm)/titanium (100 nm) bilayer, deposited on top of the SiCOH films with vacuum evaporation. The size of the metal dots is 4×10^{-4} cm^2 on the average, as measured with an optical microscope. The C-V characteristics were measured at 100 kHz on at least 12 separate metal dots with one measurement on each dot to reduce the system error by averaging the measured capacitance. The *k*-value is calculated using the following expression:

$$k = \frac{t \cdot C_{accumulation}}{A \cdot \varepsilon_0}$$

where k is the *k*-value, t is the film thickness, $C_{accumulation}$ is the averaged capacitance in the accumulation region, A is the metal dot area, and ε_0 is the vacuum permittivity. Because the

conducting area on the bottom of the sample is much larger than the top electrode, the calculated k is usually over-estimated (since A is under-estimated). Therefore, the k-values of the pristine films supplied by Intel were used to normalize our calculated k-values.

The electric field for TZDB is determined from the I-V characteristics, utilizing a setup similar to that used for the C-V characteristics, except that the LCR meter is replaced with a Keithley 6487 picoammeter. A voltage ramping rate of approximately 1 volt/second was used. The criterion for TZDB is defined as the point at which the current density exceeds 0.5 A/cm^2.

Chemical-bonding information was obtained using Fourier-transform infra-red (FTIR) spectroscopy measurements, performed with a Thermo Micro FTIR Spectrometer. The measured spectra were manually baseline-corrected one-by-one (*i.e.* based not on a generic baseline but an individual baseline for each curve). The curves were not normalized with respect to the film thickness in order to estimate the absolute number of bonds instead of their relative concentration.

Elemental composition information was found with XPS depth-profiling, as measured with a Thermo K-Alpha XPS. Only Si, C, and O could be detected with this technique. H and Cs could not be detected with XPS, because H has no core electron and Cs has too low a concentration in these films to be distinguishable from noise.

3. Results and discussion

Figure 1 Ellipsometry measured film thickness of V1 and V2 films, after each process step. Lines do not represent the processing sequence but are only used as visual aids.

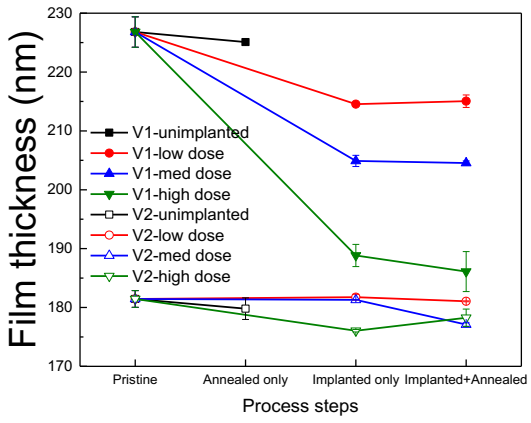

Effects of implantation and annealing on film thickness -

The results are shown in **Figure 1**. Several effects can be observed from Figure 1. Note that each line in Figure 1 represents a particular processing sequence. First, "300°C, one hour" thermal annealing only causes a very small shrinkage, about 1%, of both the pristine V1 and V2 films. This indicates that the chosen annealing condition is moderate that it does not cause film densification because the thermal budget is low enough so avoid significant chemical changes to the pristine films.

Second, for implanted-only samples, the Cs implantation causes the film thickness to shrink, and the shrinkage increases as the Cs dose increases. The only "exception" to this is that the

thickness of the V2-I-M-A (M = medium dose) sample is slightly smaller than the thickness of the V2-I-H-A (H = High Dose) sample. However, considering the extent of the error bars, this may not really be an exception. In general, the shrinkage of the V2 samples is much smaller than that of the V1 samples. This difference indicates that the thickness shrinkage may be primarily due to the presence of the porogen in the V1 film, and a corresponding lack of its presence in the V2 film.

Third, the implanted-and-annealed samples show an additional shrinkage on top of the shrinkage caused by implantation alone. The magnitude of this additional shrinkage is similar to the magnitude of shrinkage of the annealed-only samples (comparing both to their corresponding pristine samples). This indicates that the mechanisms for these two effects, one due to Cs implantation and one due to thermal annealing, can be separated.

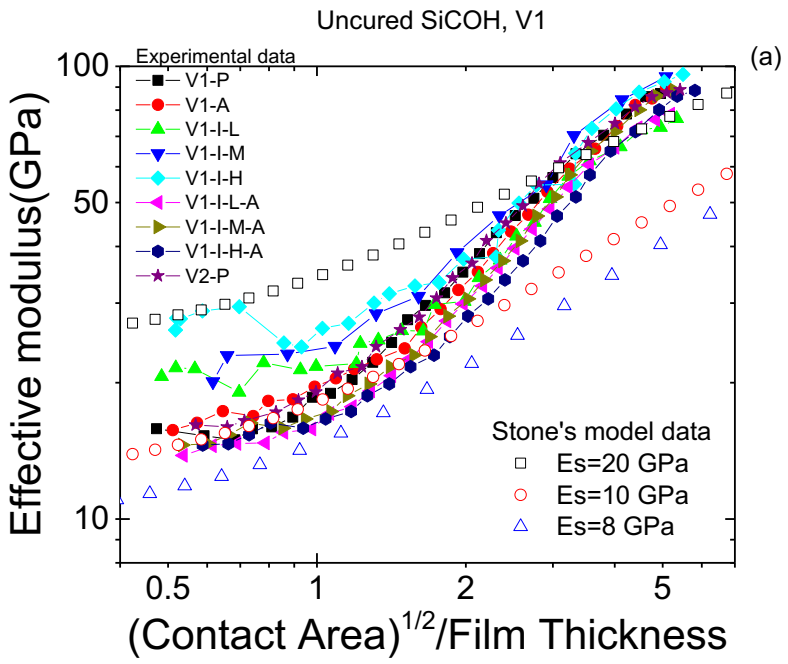
Uncured SiCOH, V1
(a)
Experimental data
V1-P
V1-A
V1-I-L
V1-I-M
V1-I-H
V1-I-L-A
V1-I-M-A
V1-I-H-A
V2-P
Stone's model data
Es=20 GPa
Es=10 GPa
Es=8 GPa
Effective modulus(GPa)
100
50
10
0.5
1
2
5
(Contact Area)^1/2/Film Thickness

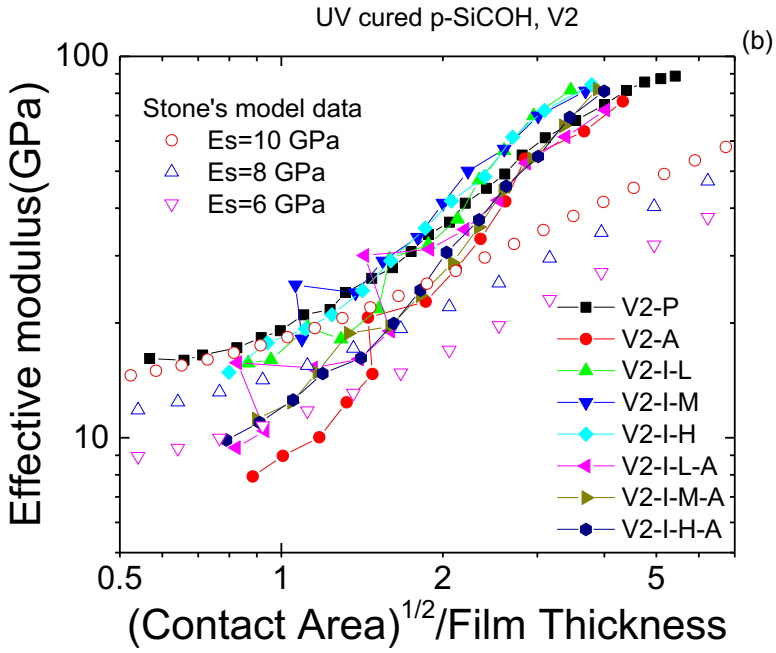

Figure 2 Effective moduli of (a) V1 series, and (b) V2 series samples measured with nano-indentation. Stone's theoretical model[34] is shown in hollow symbols. Labels: P- pristine, I-implanted, L-low dose, M-medium dose, H-high dose, A- annealed.

Effects of implantation and annealing on elastic modulus –

Figure 2 shows the effective moduli of both the V1 and V2 samples as measured with nanoindentation. A theoretical model developed by Stone,[34] which includes the contribution of

the silicon substrate into account when analyzing the measured data, is also shown as hollow points in

Figure 2. The method used to interpret this type of data has been introduced elsewhere.[26, 32] In general, the higher the curve, the better the elastic modulus. In addition, the data points for shallower indents (towards the left on the horizontal axis) reflect more of the properties of the film than those of the substrate.

It can be seen in

Figure 2(a) that the uncured V1 film is greatly strengthened by Cs implantation, which improves even more as the Cs dose increases. UV curing, on the other hand, does not show such improvement (compare V1-P with V2-P). Quantitatively, by comparing the measured data of V1-I-H (implanted-only, high dose) with the data generated using Stone's model,[34] the elastic modulus increases from about 10 GPa for the V1-P sample to about 20 GPa for the V1-I-H sample. However, there is a clear drop seen on the V1-I-H nanoindentation curve in Figure 2 when the indenter goes deeper (towards the right in the figure), indicating that the high effective modulus measured before the drop may be partially caused by surface densification during the Cs implantation process. Even so, for all three Cs doses, it is still clear that the Cs-implanted samples exhibit improved mechanical properties.

Conversely, annealing *after* implantation caused no improvement. Instead it results in a decrease in the modulus of the Cs-implanted samples. From

Figure 2(b), it can be seen that for the UV-cured V2 film, no improvement in the effective modulus was observed, either after Cs implantation or implantation followed by annealing. This is similar to our previous findings,[32] *i.e.* there was no benefit for Cs implantation in an already UV-cured film.

In a number of recent works, the improvement of mechanical properties was attributed to an increase in the Si-O-Si network structure.[22, 29, 36] We observe similar effects in this work. Gaussian peak deconvolution fitting[37] was used to separate the contributions to the FTIR spectra from the Si-O-Si cage structure, network structure, and suboxide structure.[9, 37] An example of this deconvolution, performed on sample V1-P, is shown in **Figure 3**. The inset table in the Figure shows fitted parameters for three distinct Gaussian peaks (cage, network and suboxide). Each peak has four parameters. These are: y_0-vertical base offset, x_c-horizontal center, w-peak width (twice sigma, not FWHM), and A-area under the curve. In this work, the values of fitted x_c and A are essential, because x_c indicates which of the three Si-O-Si structures a certain peak represents, and A indicates what is the proportion of this particular structure out of the total three. After fitting, the peaks can be labeled as cage, network, and suboxide according to their corresponding x_c values. The A values of each peak can then be used to calculate a ratio in the following expression:

$$\frac{A_{network}}{A_{total}} = \frac{A_{network}}{A_{cage} + A_{network} + A_{suboxide}}$$

Thus for each sample there is such a ratio, which can be used as a measure of its mechanical

properties.

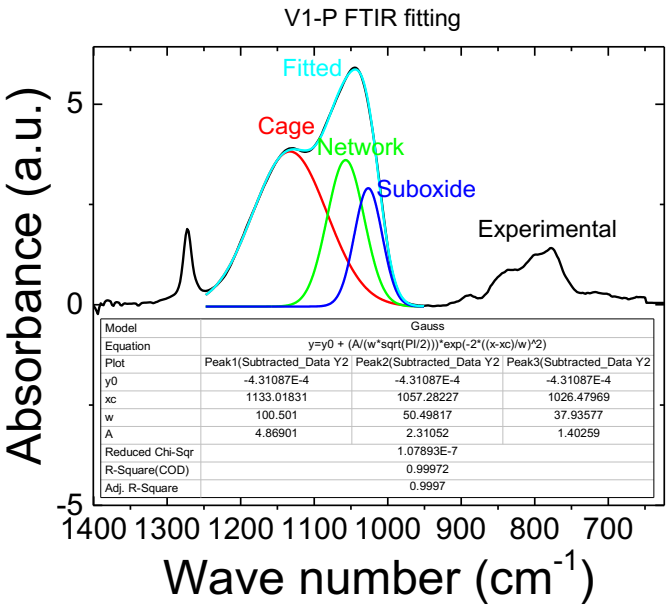

Model	Gauss		
Equation	y=y0 + (A/(w*sqrt(PI/2)))*exp(-2*((x-xc)/w)^2)		
Plot	Peak1(Subtracted_Data Y2	Peak2(Subtracted_Data Y2	Peak3(Subtracted_Data Y2
y0	-4.31087E-4	-4.31087E-4	-4.31087E-4
xc	1133.01831	1057.28227	1026.47969
w	100.501	50.49817	37.93577
A	4.86901	2.31052	1.40259
Reduced Chi-Sqr	1.07893E-7		
R-Square(COD)	0.99972		
Adj. R-Square	0.9997		

Figure 3 Example of FTIR spectral deconvolution of the Si-O-Si structure.

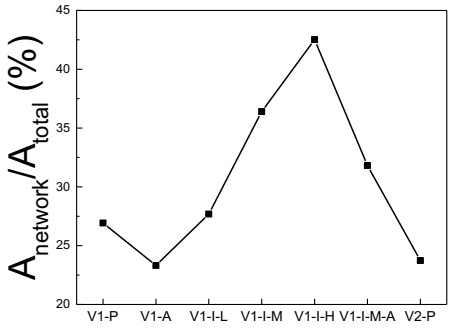

Figure 4 FTIR area-to-area ratio $A_{network}/A_{total}$ of various samples. Labels: P-pristine, I-implanted, L-low dose,

M-medium dose, H-high dose, A-annealed. The line does not necessarily represent the process sequence.

The ratios for the various samples are shown in **Figure 4**. It can be seen that the ratio increases after Cs implantation, and it increases further when the Cs dose increases. On the other hand, thermal annealing, either by itself or after Cs implantation, shows a decrease of this ratio. UV curing by itself also decreases this ratio. These findings are consistent with the measured elastic moduli in

Figure 2. That is, the increase of the modulus is consistent with the increase in the network structure.

Comment [WL1]: What do you mean here? Which figure is cut off? I don't see one missing.

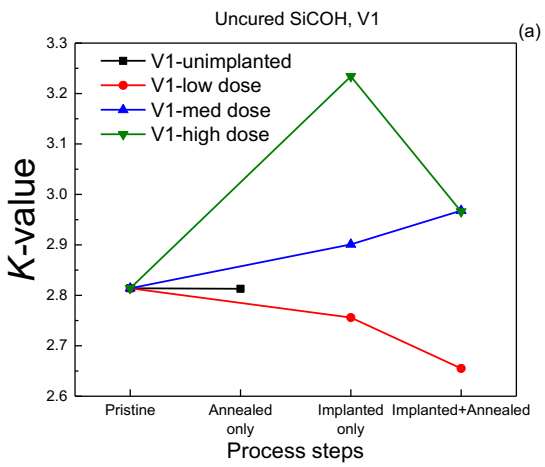

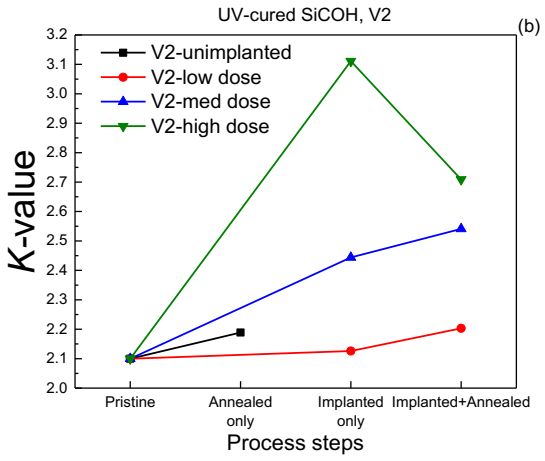

Figure 5 The *k*-values of (a) V1, (b) V2 samples after each process step.

Effects of implantation and annealing on k-values –

The normalized *k*-values are shown in **Figure 5**. The relative changes of the *k*-values of the annealed only, implanted only, and implanted-and-annealed samples with respect to their corresponding pristine samples are shown in **Figure 6**.

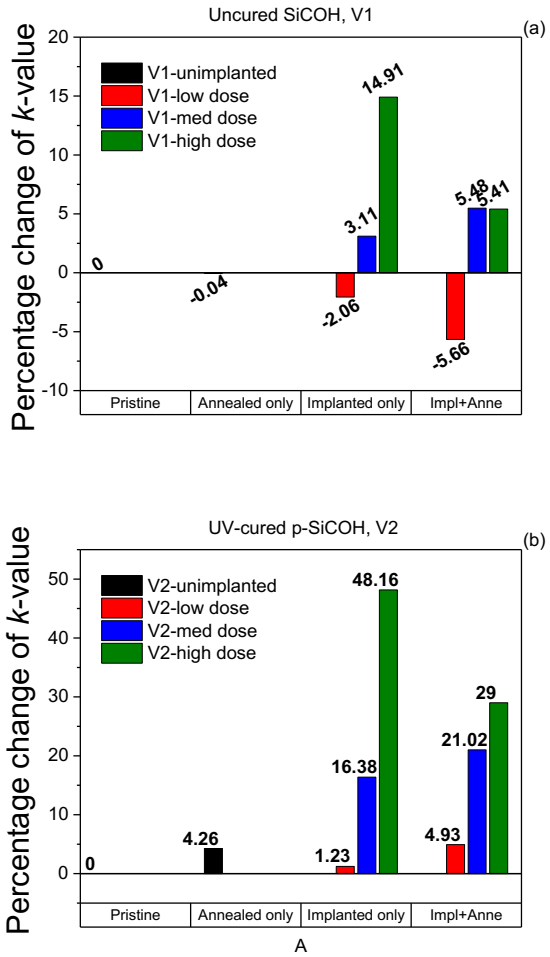

Figure 6 Relative change in percentage of the *k*-value of processed (a) V1, and (b) V2 samples with respect to their corresponding pristine sample's *k*-value

From both Figure 5 and Figure 6, several observations about the *k*-value changes can be made. First, the *k*-value of V1 film is affected very little from thermal annealing alone, while that

of the V2 film is increased by about 4%.

Second, Cs-implanted samples do not always show an increased *k*-value, which is different from the results previously presented for non-porous SiCOH, in which Cs implantation caused an increase in the *k*-value no matter how high the Cs dose is.[32] For the V1 samples, low-dose Cs implantation actually lowers its *k*-value slightly. For medium and high dose, the *k*-values of all samples increase as the Cs dose increased. In addition, the porogen-embedded V1 films show a much smaller increase of *k*-value compared with the UV-cured V2 film. This is similar to what was found in our non-porous SiCOH work,[32] where implanting Cs into UV-cured SiCOH caused a significant increase of the *k* value.

Third, in many cases, the percentage of the *k*-value increase is less for the implanted-and-annealed samples compared with their corresponding implanted-only samples. This is the opposite effect compared with what was observed in our non-porous SiCOH work,[32] in which thermal annealing always caused the *k*-value to increase.

To explain this in the non-porous SiCOH work,[32] we stated that the samples were undesirably oxidized during furnace annealing, due to the presence of oxygen in the atmosphere contacting the still-hot samples after annealing. In this work, however, no such oxidation occurred because a vacuum heater was used to perform the annealing instead of the furnace. Thus, in this work, the samples can be sufficiently cooled down to room temperature before making contact with the atmosphere. In this case, the vacuum annealing seems to be able to partially mitigate the *k*-value increase caused by Cs implantation, especially for medium and

high Cs doses. This might be due to two reasons. One, some porogen can be removed after annealing, leaving pores behind that reduce the *k*-value. Two, water which was absorbed after Cs implantation can be driven out during vacuum annealing, which also helps to reduce the *k*-value.

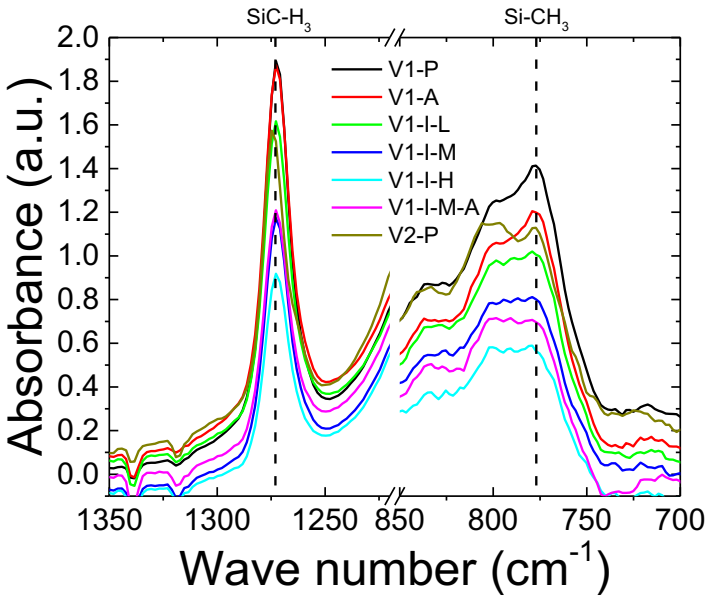

Figure 7 FTIR spectra of the SiC-H_3 bond and the Si-CH_3 bond of the V1 I and I-A samples compared with pristine V1 (uncured) and V2 (UV-cured) samples. Labels: P- pristine, I-implanted, L-low dose, M-medium dose, H-high dose, A- annealed.

In order to determine the mechanism causing the observed change of *k*-value, the FTIR spectra of the V1-series samples (Pristine, implanted only, and implanted-and-annealed), are shown in **Figure 7**. For comparison, the FTIR spectrum of the UV-cured V2-P (Pristine) sample

is also shown in Figure 7. It can be seen that for both the implanted-only and the implanted-and-annealed samples, there is a clear carbon loss,[37] which increases as the Cs dose increases. This explains the increase of the *k*-values.

On the other hand, compared with the *k*-value increase for either low, medium, or high Cs doses in our non-porous SiCOH work,[32] the *k*-value increase for porous SiCOH with the corresponding dose is suppressed in the porogen-embedded V1 film. A plausible explanation is that this is attributed to pore creation in the film from the implanted Cs ions. This is especially likely near the surface of the film.

One piece of evidence for this is shown in the FTIR spectra in **Figure 8**. In Figure 8 it can be seen that the -CH_x peaks of the implanted-only and implanted-and-annealed samples decrease, and this decrease is similar to the effect produced by UV curing, *i.e.* the difference between the V1-P and the V2-P samples. With a higher Cs dose, these peaks decrease more. Thermal annealing also leads to a decrease of these peaks, which supports our aforementioned explanation that annealing can remove the porogen. It is widely accepted that these -CH_x peaks are indicators of the porogen amount left inside the film.[22, 36] Therefore, from Figure 8, we deduce that the implanted Cs ions, either by themselves or combined with subsequent annealing, have resulted in partial removal of the porogen that was embedded in the pristine film, resulting in pore creation. This effect explains the suppression of the *k*-value increase, compared with the non-porous SiCOH case.[32]

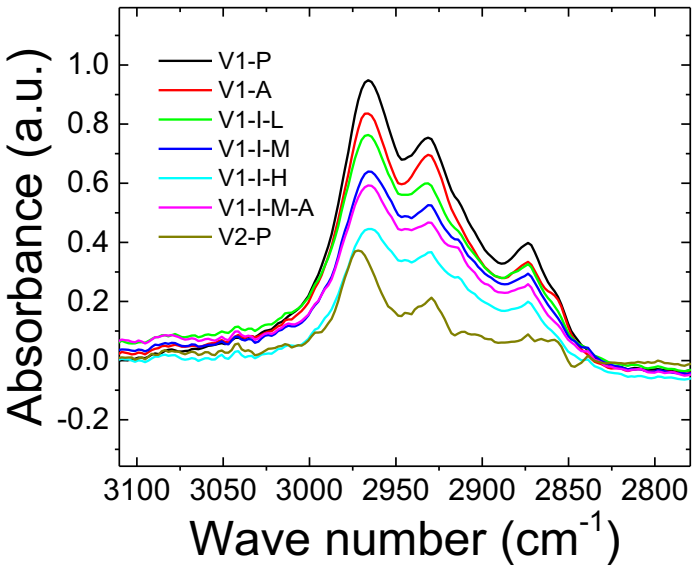

Figure 8 FTIR spectra of $-CH_x$ (porogen-related) peaks of V1 I and IA samples compared with pristine V1 (uncured) and V2 (UV-cured) samples, Labels: P- pristine, I-implanted, L-low dose, M-medium dose, H-high dose, A-annealed.

Additional support for this hypothesis can be found from the XPS depth profile. **Figure 9** shows the XPS depth profiles of pristine V1 and V2 samples, as well as that for Cs-implanted V1 samples. It can be seen from Figure 9 that, similarly to what was found in the non-porous SiCOH work,[32] carbon loss within approximately the top 40% of the film near the surface can be observed. The degree of this loss is stronger as the Cs dose increases. In addition, a corresponding increase in oxygen can be observed in the same region.

However, there is a different phenomenon in this work which must be considered. It is related to silicon. Unlike what was found for non-porous SiCOH,[32] where the silicon composition was almost unchanged by Cs implantation, in Figure 9(a) it can be seen that the Si composition in the aforementioned top 40% of the film thickness region increases. In addition, the degree of this increase is stronger as the Cs dose increases. Since Si atoms are believed to be more difficult to remove from the film, we deduce that this change in composition is a reflection of losing porogen material, which, to the best of our knowledge, contains carbon, oxygen, and hydrogen, but not silicon. Note that XPS measurements do not give the absolute but only the relative elemental concentrations, thus removing other elements than silicon results in an increase of the relative concentration of silicon. Therefore, this observation supports our hypothesis of porogen removal due to Cs implantation.

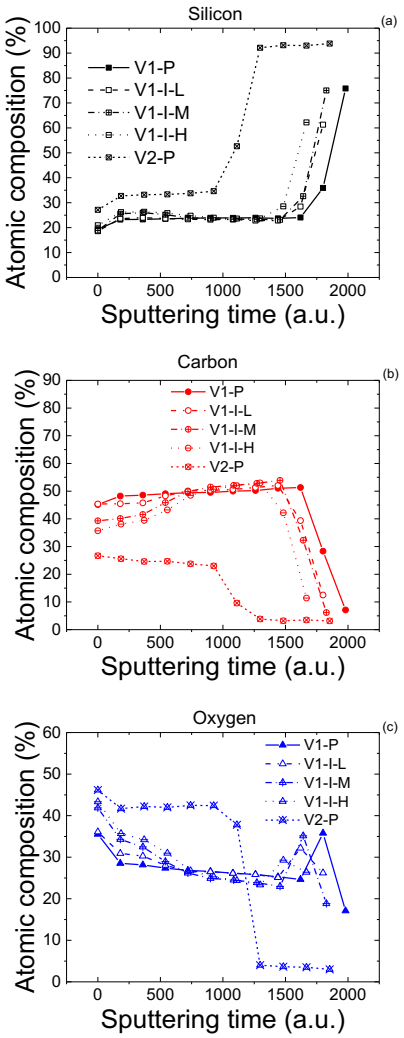

Figure 9 XPS depth profiles of (a) silicon, (b) carbon, and (c) oxygen atoms of V1 series of samples. Pristine V2 sample is also shown for comparison. Labels: P- pristine, I-implanted, L-low dose, M-medium dose, H-high dose, A- annealed.

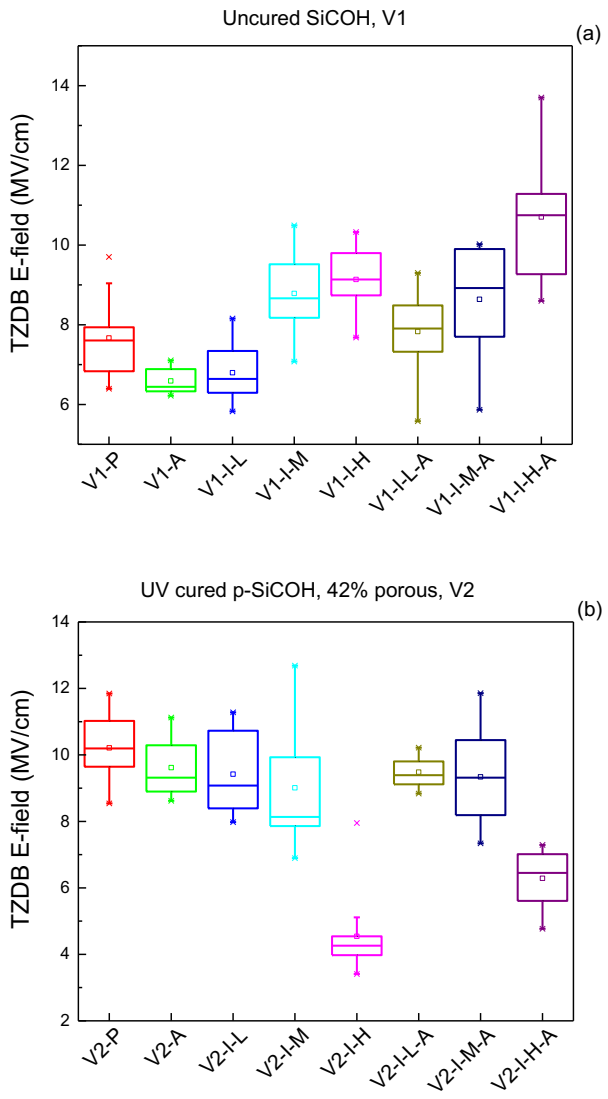

Figure 10 Box-plots of the TZDB electric field of (a) V1, and (b) V2 samples. Labels: P- pristine, I-implanted, L-low dose, M-medium dose, H-high dose, A- annealed.

Effects of implantation and annealing on TZDB field strength –

Figure 10 shows box-plots of the TZDB electric-field statistics for all the samples, measured with I-V characteristics at room temperature. The box-plot statistics are based on at least 12 measurements on separate metal dots, one measurement on each dot. Several observations can be found from Figure 10. First, the annealed-only samples do not show any improvement (increase) in the TZDB field as compared with their corresponding pristine samples. In fact, for both V1 and V2 films, the annealed-only samples show *lower* TZDB fields.

Second, for uncured V1 films, the medium and high-dose Cs implantations do increase the TZDB field, while the low-dose implantations do not show this effect. Conversely, for the already UV-cured V2 film, almost all of the Cs-implanted samples show lower TZDB fields. This decrease is more significant when the Cs dose is higher. Third, annealing after Cs implantation in general either improves or holds the TZDB field compared with that of the corresponding implanted-only samples.

The improvement of TZDB due to Cs implantation may be explained by film densification, which was observed with the thickness measurements. In fact, some Cs-implanted uncured samples show equal or better TZDB fields compared with the corresponding UV-cured samples. One example is V1-I-H-A compared with V2-P. The additional improvement due to subsequent annealing can be explained by considering the effect of high-temperature-enhanced diffusion of the implanted Cs ions, which redistributes the Cs ions more uniformly, thus decreasing the local

electric-field peak.

4. Conclusion

In conclusion, we have found that Cs implantation in porogen-embedded SiCOH samples exhibits benefits such as improving the elastic modulus, improving TZDB, and partially removing porogen to make pores. These effects are all beneficial for the requirements for low-*k* dielectrics. In addition, the undesirable *k*-value increase can be suppressed to a relatively low value compared with the increase in the case of non-porous SiCOH. This phenomenon suggests that Cs implantation of porogen-embedded SiCOH may be more useful than implantation of non-porous SiCOH. However, implanting Cs into UV-cured p-SiCOH leads to an unacceptable increase of the *k*-value, while it does not increase the elastic modulus.

Acknowledgement

This work was supported by the National Science Foundation under Grant CBET-1066231 and by the Semiconductor Research Corporation under Contract 2012-KJ-2359.

References

[1] G. E. Moore, *Electronics Magazine* **1965**, *38*.

[2] M. T. Bohr, presented at International Electron Devices Meeting **1995**.

[3] A. Grill, V. Patel, K. L. Saenger, C. J. Jahnes, S. A. Cohen, A. G. Schrott, *Mater Res Soc Symp P* **1997**, *443*, 155.

[4] M. G. Albrecht, C. Blanchette, *Journal of the Electrochemical Society* **1998**, *145*, 4019.

[5] A. Grill, V. Patel, C. Jahnes, *Journal of the Electrochemical Society* **1998**, *145*, 1649.

[6] Y. K. Lee, S. P. Murarka, *J Mater Sci* **1998**, *33*, 5423.

[7] A. Grill, L. Perraud, V. Patel, C. Jahnes, S. Cohen, presented at MRS Proceedings **1999**.

[8] T. Furusawa, N. Sakuma, D. Ryuzaki, S. Kondo, K.-i. Takeda, S.-t. Machida, K. Hinode, presented at Interconnect Technology Conference, 2000. Proceedings of the IEEE 2000 International **2000**.

[9] K. Maex, M. R. Baklanov, D. Shamiryan, F. Iacopi, S. H. Brongersma, Z. S. Yanovitskaya, *Journal of Applied Physics* **2003**, *93*, 8793.

[10] L. A. Clevenger, M. Yoon, D. Edelstein, A. Cowley, C. Davis, B. Agarwala, P. Biolsi, K. Chanda, T. Cohen, W. Cote, M. Cullinan, T. Dalton, S. Das, P. Davis, J. Demarest, D. Dunn, C. Dziobkowski, L. Economikos, R. Filippi, J. Fitzsimmons, P. Flaitz, N. Fuller, T. Gates, J. Gill, A. Grill, D. Hawken, R. Joy, N. Klymko, M. Lane, S. Law, W. Landers, N. Le, W. K. Li, Y. H. Lin, E. Liniger, H. Liu, W. Liu, X. Liu, D. Llera-Hurlburt, C. H. Low, S. Malhotra, G. Matusiewicz, S. Moskowitz, C. Muzzy, D. Nguyen, S. Pal, C. Parks, V. Ramachandran, H. Rathore, D. Restaino, B. Rhoads, T. Shaw, J. Schmitt, A. Simon, J. Tan, T. Tang, S. Tempest, T. Van Kleeck, S. Vogt, R. Wagner, W. Y. Wang, Y. Y. Wang, W. Wille, J. Wright, C. C. Yang, T. Ivers, *Advanced Metallization Conference 2004 (Amc 2004)* **2004**, 27.

[11] A. Grill, D. Edelstein, D. Restaino, M. Lane, S. Gates, E. Liniger, T. Shaw, X. H. Liu, D. Klaus, V. Patel, S. Cohen, E. Simonyi, N. Klymko, S. Lane, K. Ida, S. Vogt, T. Van Kleeck, C. Davis, M. Ono, T. Nogami, T. Ivers, *Proceedings of the Ieee 2004 International Interconnect Technology Conference* **2004**, DOI: Doi 10.1109/Iitc.2004.134568254.

[12] International Technology Roadmap for Semiconductors (ITRS 2009), http://www.itrs.net/Links/2009ITRS/Home2009.htm, accessed.

[13] M. R. Baklanov, K. Maex, *Philos T R Soc A* **2006**, *364*, 201.

[14] S.-I. Nakao, J. Ushio, T. Ohno, T. Hamada, Y. Kamigaki, M. Kato, K. Yoneda, S. Kondo, N. Kobayashi, presented at International Interconnect Technology Conference, Burlingame, CA **2006**.

[15] S. Sankaran, S. Arai, R. Augur, M. Beck, G. Biery, T. Bolom, G. Bonilla, O. Bravo, K. Chanda, M. Chae, F. Chen, L. Clevenger, S. Cohen, A. Cowley, P. Davis, J. Demarest, J. Doyle, C. Dimitrakopoulos, L. Economikos, D. Edelstein, M. Farooq, R. Filippi, J. Fitzsimmons, N. Fuller, S. M. Gates, S. E. Greco, A. Grill, S. Grunow, R. Hannon, K. Ida, D. Jung, E. Kaltalioglu, M. Kelling, T. Ko, K. Kumar, C. Labelle, H. Landis, M. W. Lane,

W. Landers, M. Lee, W. Li, E. Liniger, X. Liu, J. R. Lloyd, W. Liu, N. Lustig, K. Malone, S. Marokkey, G. Matusiewicz, P. S. McLaughlin, P. V. McLaughlin, S. Mehta, I. Melville, K. Miyata, B. Moon, S. Nitta, D. Nguyen, L. Nicholson, D. Nielsen, P. Ong, K. Patel, V. Patel, W. Park, J. Pellerin, S. Ponoth, K. Petrarca, D. Rath, D. Restaino, S. Rhee, E. T. Ryan, H. Shoba, A. Simon, E. Simonyi, T. M. Shaw, T. Spooner, T. Standaert, J. Sucharitaves, C. Tian, H. Wendt, J. Werking, J. Widodo, L. Wiggins, R. Wisnieff, T. Ivers, I. S. T. Grp, *Int El Devices Meet* **2006**, 89.

[16] A. Grill, *Annu Rev Mater Res* **2009**, *39*, 49.

[17] A. Grill, *J Vac Sci Technol B* **2016**, *34*.

[18] A. Grill, V. Patel, K. P. Rodbell, E. Huang, M. R. Baklanov, K. P. Mogilnikov, M. Toney, H. C. Kim, *Journal of Applied Physics* **2003**, *94*, 3427.

[19] F. Iacopi, C. Waldfried, K. Houthoofd, E. P. Guyer, D. M. Gage, G. Carlotti, Y. Travaly, T. Abell, O. Escorcia, G. Beyer, I. Berry, R. H. Dauskardt, K. Maex, *Advanced Metallization Conference 2005 (AMC 2005)* **2006**, 247.

[20] A. Zenasni, V. Jousseaume, P. Holliger, L. Favennec, O. Gourhant, P. Maury, G. Gerbaud, *Journal of Applied Physics* **2007**, *102*, 094107.

[21] D. M. Gage, E. P. Guyer, J. F. Stebbins, Z. Cui, A. Al-Bayati, A. Demos, K. P. MacWilliams, R. H. Dauskardt, *Proceedings of the IEEE 2006 International Interconnect Technology Conference* **2006**, 149.

[22] P. Verdonck, D. De Roest, S. Kaneko, R. Caluwaerts, N. Tsuji, K. Matsushita, N. Kemeling, Y. Travaly, H. Sprey, M. Schaekers, G. Beyer, *Surface and Coatings Technology* **2007**, *201*, 9264.

[23] Y. Shioya, T. Ohdaira, R. Suzuki, Y. Seino, K. Omote, *J Non-Cryst Solids* **2008**, *354*, 2973.

[24] J. B. Vella, I. S. Adhihetty, K. Junker, A. A. Volinsky, *International Journal of Fracture* **2003**, *120*, 487.

[25] L. G. Wang, M. Ganor, S. I. Rokhlin, A. Grill, *Journal of Materials Research* **2005**, *20*, 2080.

[26] X. Guo, J. E. Jakes, M. T. Nichols, S. Banna, Y. Nishi, J. L. Shohet, *Journal of Applied Physics* **2013**, *114*, 084103.

[27] K. E. Petersen, *IEEE Transactions on Electron Devices* **1978**, *25*, 1241.

[28] A. Grill, S. M. Gates, T. E. Ryan, S. V. Nguyen, D. Priyadarshini, *Appl Phys Rev* **2014**, *1*, 011306.

[29] A. M. Urbanowicz, K. Vanstreels, P. Verdonck, D. Shamiryan, S. De Gendt, M. R. Baklanov, *Journal of Applied Physics* **2010**, *107*, 104122.

[30] X. Guo, J. E. Jakes, S. Banna, Y. Nishi, J. L. Shohet, *Journal of Applied Physics* **2014**, *116*.

[31] H. Zheng, X. Guo, D. Pei, W. Li, J. Blatz, K. Hsu, D. Benjamin, Y.-H. Lin, H.-S. Fung, C.-C. Chen, Y. Nishi, J. L. Shohet, *Applied Physics Letters* **2016**, *108*, 242906.

[32] W. Li, D. Pei, X. Guo, M. K. Cheng, S. Lee, Q. Lin, S. W. King, J. L. Shohet, *Applied Physics Letters* **2016**, *108*, 202901.

[33] J. F. Ziegler, M. D. Ziegler, J. P. Biersack, *Nucl Instrum Meth B* **2010**, *268*, 1818.
[34] D. S. Stone, *Journal of Materials Research* **1998**, *13*, 3207.
[35] P. Verdonck, E. Van Besien, K. Vanstreels, C. Trompoukis, A. Urbanowicz, D. De Roest, M. R. Baklanov, *Japanese Journal of Applied Physics* **2011**, *50*.
[36] O. Gourhant, G. Gerbaud, A. Zenasni, L. Favennec, P. Gonon, V. Jousseaume, *Journal of Applied Physics* **2010**, *108*, 124105.
[37] A. Grill, D. A. Neumayer, *Journal of Applied Physics* **2003**, *94*, 6697.